Koene, Ivar; Viitala, Raine; Kuosmanen, Petri

Vibration monitoring of a large rotor utilizing internet of things based on-shaft MEMS accelerometer with inverse encoder

Published in:
12th International Conference on Vibrations in Rotating Machinery

Published: 01/01/2020

Document Version
Publisher's PDF, also known as Version of record

12th International Conference on Vibrations in Rotating Machinery - Institution of Mechanical Engineers, ISBN 978-0-367-67742-8

Vibration monitoring of a large rotor utilizing internet of things based on-shaft MEMS accelerometer with inverse encoder

I. Koene, R. Viitala, P. Kuosmanen

Department of Mechanical Engineering, Aalto University, Finland

ABSTRACT

Typically, accelerometer-based vibration measurements of rotating machinery are conducted with sensors mounted to a static part of the machine. Now, with increasing accuracy of compact and low powered microelectromechanical systems (MEMS) accelerometers, on-shaft vibration measurements have become an interesting research topic. MEMS sensors are optimal for internet of things (IoT) applications and wireless measurements, which makes on-shaft measurements more convenient. However, typically in wireless applications, the sample clock is time-based, and thus the data is not bound to the phase of the rotating rotor. In this research, a novel wireless sensor unit with an inverse encoder is mounted to the end of a large rotor to investigate the dynamic behavior of the rotor. In addition, a method to separate the vertical and horizontal vibration from the sensor data is studied.

1 INTRODUCTION

Vibration measurement is a crucial part of the condition monitoring of a rotating machine and accelerometers are commonly used to measure the vibrations. Typically, these sensors are wired piezoelectric accelerometers, and they are mounted to a static part of the machine, such as a bearing housing or frame (1)–(5). However, in recent years cost-effective, compact and low powered microelectromechanical systems (MEMS) accelerometers have become a popular option to replace the piezoelectric sensors. Several different types of MEMS accelerometer sensing schemes have been developed, such as piezoresistive (6) and capacitive (7), (8), (9), (10) based sensing elements. Capacitive sensing elements are commonly used due to their good noise performance, high sensitivity and low temperature sensitivity (7). Piezoelectric and MEMS accelerometers have been studied and compared to determine whether the MEMS sensor can measure the same phenomenon as a piezoelectric sensor (1), (2), (4), (5), (11). MEMS accelerometers have shown promising results, and in many situations, the piezoelectric accelerometer could be replaced with a MEMS sensor. However, the noise level has been higher compared to the piezoelectric accelerometers, as Koene et al. (4) pointed out in their research.

The low power consumption of the MEMS sensors enables using a battery as a power source. With a battery as a power source, wireless data transfer is beneficial as the cables can be eliminated. The wireless measurement gives a new opportunity to measure rotor behavior by mounting the sensors directly to the rotating part of the machine. Elnady et al. (12), (13), Jiménez et al. (14) and Feng et al. (15) have studied condition monitoring of a rotating machine by mounting a MEMS accelerometer to the rotor. Elnady et al. (12), (13) mounted a two-axis accelerometer to the surface of the rotor, as well as two one-axis accelerometers to the bearing housing of the same rotor, to study lateral vibrations. Because the sensor was not aligned with the central axis of the rotor, the accelerometer measured radial and tangential accelerations. They conducted a sweep measurement and noticed that the vibration peaks did not occur at the same

frequency in the bearing housing accelerometer data and on-shaft accelerometer data. In the on-shaft accelerometer data, the vibration peaks were observed at two different frequencies, which had a mean frequency coinciding with the corresponding peak frequency from the bearing housing (12). Jimémez et al. (14) observed the same phenomenon when they did impact tests with their test rotor.

Jimémez et al. (14) aligned a two-axis MEMS accelerometer with the rotor central axis. They analyzed the measurement data to solve the radius of the rotor orbit and the velocity of the rotor. They also conducted impact measurements to observe the natural frequency of the system. Feng et al. (15) studied compressor condition monitoring by mounting a MEMS accelerometer to the flywheel of the compressor. They studied a method on how to eliminate the gravitational acceleration from the rotating accelerometer data. Their results indicate that the on-shaft sensor can be used to detect the common fault types of their test compressor. In addition to rotor condition monitoring, wind turbine condition monitoring has adopted piezoelectric and MEMS accelerometers (16)–(19). With wind turbines, the accelerometers can be mounted to the wind turbine frame (18), (19), or to the rotating blades itself (16)–(18). Typically, in these cases, several accelerometers are used simultaneously, which requires designing and studying sensor networks (18), (19). It is also possible to adopt these sensor networks to another rotating machine condition monitoring application, where monitoring several rotating parts is required.

This paper presents a novel on-shaft MEMS accelerometer unit, which has an inverse encoder, and a novel method to separate the vertical and horizontal vibration from the accelerometer data. The inverse encoder signifies an encoder, which rotates with the rotor, and the encoder shaft is mounted to a static part of the machine. The code wheel of the encoder is mounted to the encoder shaft; hence the code wheel is fixed in the Earth's coordinate system and does not rotate as with typical encoders. In the inverse encoder, the light sensors measuring the code wheel rotates with the rotor, which eliminates the need for slip rings when using an encoder as a sample clock with an on-shaft sensor. The internal timer of the sensor unit can be used as a sample clock as well, which enables the possibility to study two different sampling clock methods.

2 METHODS

2.1 Proposed sensor unit and reference sensor

The proposed sensor unit consists of ESP32 internet of things (IoT) platform (Espressif Systems), AD7682 analog to digital converter (ADC) (Analog Devices), ADXL354 3-axis MEMS accelerometer (Analog Devices) and AMT102 encoder (CUI devices) with 1024 pulses per revolution and reference pulse, which occurs once per revolution. Figure 1 presents the sensor unit. The specification of the parts can be found from Tables 1, 2 and 3. The measurement range of ADXL354 in the measurements was ±8 g, which signifies the sensitivity of 100 mV/g. The sensor unit can also be defined to use a 10 kHz time-based sample clock (TBSC) for the measurement instead of the encoder. The TBSC was used to study the phase tracking ability of the sensor unit when the phase information was purely deducted using the MEMS data, which shows the direction of gravity. In these comparisons, the phase accuracy was compared to the inverse encoder data.

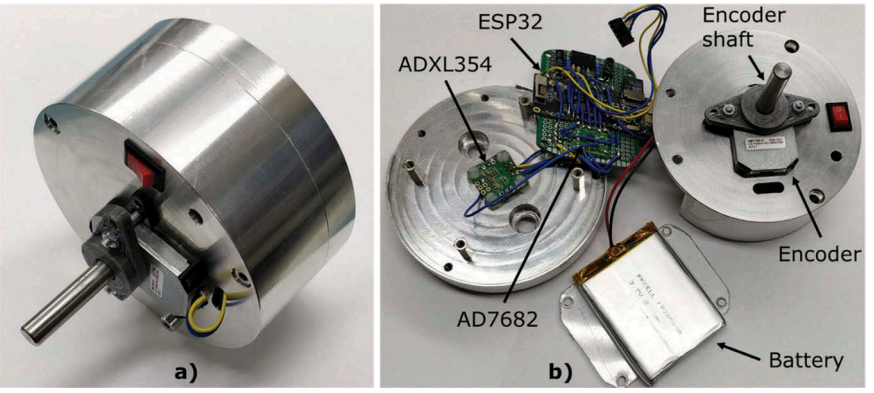

Figure 1. A) Sensor unit and b) components of the sensor unit.

To validate the measurements, a similar IoT sensor, which is verified by Koene et al. (4), was used. It had ADXL355 MEMS accelerometer, which has the same sensing elements as in ADXL354. Specifications of ADXL355 are presented in Table 3, and the same measurement range was used as with the ADXL354.

Table 1. Specifications of ESP32 IoT platform.

Specifications	**ESP32**
Microcontroller Unit	Tensilica Xtensa 32-bit LX6
Cores	2
Clock frequency (MHz)	240
SRAM (KiB)	520
802.11 b/g/n WI-FI	HT40
GPIO	36
SPI/I2C interfaces	4/2

Table 2. Specifications of AD7682 ADC.

Specifications	**AD7682**
Channels	4
Resolution	16 bits
Throughput	250 kS/s
Interface	SPI

Table 3. Specifications of ADXL354 and ADXL355 accelerometers. Used values are bolded.

Specifications	ADXL354	ADXL355
Measurement range	±2/**8** g	±2/4/**8** g
Axis	3	3
Bandwidth	1500 Hz	1000 Hz
Sensitivity	400/**100** mV/g	3.9/7.8/**15.6** µg/LSB

2.2 Test setup

Tests were conducted with full-size paper machine roll, which weighs around 700 kg and is 5 meters long. The sensor unit was mounted to the rotor end, and the reference sensor was mounted to the bearing housing. Figure 2 a) presents the test rotor, and Figure 2 b) presents the sensor setup.

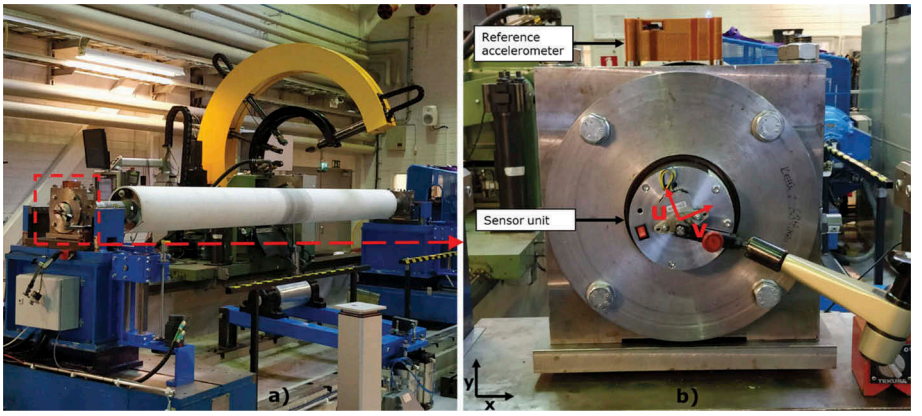

Figure 2. A) Test rotor, which weighs around 700 kg and is 5 meters long. b) Sensor setup with the sensor unit and reference sensor. The coordinate system with u- and v-axis indicate the orientation of two of the axes of the MEMS accelerometer inside the sensor unit. One axis of the MEMS accelerometer was coaxial with the axis of the rotor, but it was not used during the present study.

The measurements were done with a rotor velocity of 500 rpm (8.33 Hz), and at least 100 rounds were measured. Two measurements were made with the sensor unit: one with the encoder-based sample clock (EBSC) and one with the time-based sample clock (TBSC). During both measurements, the reference sensor was measuring simultaneously as well.t

2.3 Data analyses

In the case of TBSC measurement, the rotor phase was calculated from the gravitational component of the signal from both u- and v-axis. The calculation process is presented below and in Figure 3 as a block diagram.

1. Lowpass filter the frequencies above the rotation speed from the data
2. Determine the phase of a measurement sample with the following equations:

$$a(\alpha) = a_u(n) \cdot \cos(\alpha) + a_v(n) \cdot \sin(\alpha) \quad (1)$$

$$\alpha(n) = \arg\max_{\alpha}(a(\alpha)) \quad (2)$$

Where a_u is the u-axis acceleration value, a_v is the v-axis acceleration value, a is the angle and n is the sample number. The equation (2) finds the a value, which has the highest acceleration based on equation (1) and that a is the phase of the sample. The phase is calculated with 0.1 degree accuracy.

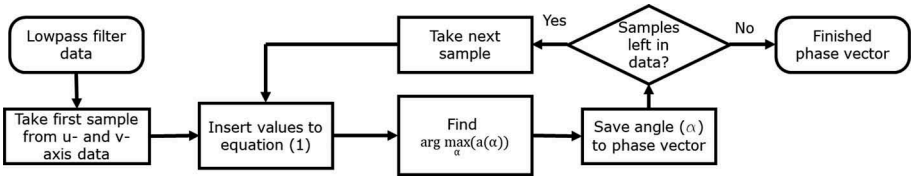

Figure 3. Method how to calculate a phase with the gravitation component of the sensor data.

Typically, lateral vibrations are measured in horizontal and vertical directions; however, in a case where the sensor rotates with the rotor, the sensor axis direction does not stay constant in the Earth's coordinate system. Hence, here is presented a method to separate the horizontal and vertical vibration from rotating sensor data with a rotation matrix:

$$\begin{bmatrix} x(n) \\ y(n) \end{bmatrix} = \begin{bmatrix} \cos(\alpha(n)) & -\sin(\alpha(n)) \\ \sin(\alpha(n)) & \cos(\alpha(n)) \end{bmatrix} \cdot \begin{bmatrix} a_u(n) \\ a_v(n) \end{bmatrix} \quad (3)$$

Where x is horizontal vibration, y is vertical vibration, a is the phase, a_u and a_v are the sensor data, and n is the sample number. The sensor axis u and v are marked in Figure 2 b). The vibration frequencies of the vertical and horizontal data were calculated with fast Fourier transform (FFT) (20).

2.4 Calibration

The sensor unit was calibrated after mounting it to the rotor by utilizing the gravitation. The calibration revealed the relation between the ADC output and the acceleration. Calibration measurement was made by rotating the test rotor 100 rounds with 10 rpm velocity. The encoder was used as a sample clock. Because the sensor was aligned with the rotor central axis and the rotor was rotated with a very low velocity, the only significant acceleration component affecting the sensor was the gravitation. The sensor was calibrated by analyzing the measurement data, as presented in Figure 4 and below:

1. Calculate one round average from the ADC output
2. Find the maximum, minimum and mean values for the one round average
    a. The maximum value is equal to 1 g
    b. The minimum value is equal to -1 g
    c. The mean value is equal to 0 g

3. Calculate the conversion coefficient to convert the ADC output to m/s^2 with the following equation:

$$k = \frac{9.81 \frac{m}{s^2} \times 2}{max - min} \tag{4}$$

Where max is the axis maximum value and min is the axis minimum value. The conversion coefficient is calculated to both u- and v-axis. The final equation to convert the ADC output to m/s^2 is for the u-axis:

$$a_u(n) = (ADC_u(n) - mean_u) \times k_u = (ADC_u(n) - 32702) \times 0.0028 \tag{5}$$

Where ADC_u is the u-axis ADC output, $mean_u$ is the u-axis mean value, k_u is the u-axis conversion coefficient and n is the sample number. For v-axis, the equation is as follows:

$$a_v(n) = (ADC_v(n) - mean_v) \times k_v = (ADC_v(n) - 32737) \times 0.0027 \tag{6}$$

Where ADC_v is the v-axis ADC output, $mean_v$ is the v-axis mean value, k_v is the v-axis conversion coefficient and n is the sample number. The $mean_u$ and $mean_v$, and k_u and k_v values are calculated from the calibration measurement data and those same values were used to convert the measurement data from the ADC output to m/s^2. The phase offset of the encoder is determined by using the maximum value of the one round average, which indicates a 90-degree phase.

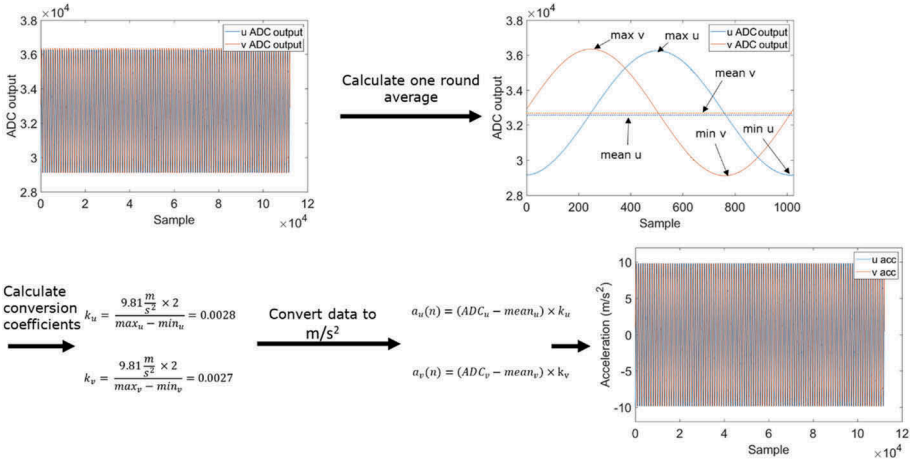

Figure 4. Calibration process and conversion from ADC values to acceleration.

3 RESULTS

Figures from 5 to 11 presents the test results from the 500 rpm measurements. The sensor unit measurement results are presented in three different ways, which are listed below:

1. measurements with the encoder-based sample clock (EBSC) and encoder-based phase (Figures 5 a), 6 a), 7 a), 8 a), 9 a) and 11 a)),
2. measurements with the time-based sample clock (TBSC) and gravity-based phase (Figures 8 b) and 9 b)),
3. and measurements with the encoder-based sample clock (EBSC) and gravity-based phase (Figure 11 b)).

The last category is used to compare how two differently determined phases effect to the coordinate transformation of the same measurement data.

3.1 Encoder-based sample clock measurement

Figures 5 and 6 present the sensor unit data with the EBSC and encoder-based phase after the coordinate transformation, as well as the reference sensor data. In Figure 5, the results are similar in the horizontal direction (x-axis). The same vibration peaks can be observed from both the proposed and reference sensor data, and the horizontal natural frequency is visible as well, being approximately 20.9 Hz. However, the amplitudes differ from each other.

When comparing the vertical vibrations (Figure 6), there are more differences. The amplitudes have more deviation between the sensors: the reference sensor has approximately 20 times lower highest vibration peak than the sensor unit data. The vertical natural frequency is approximately 29.2 Hz, and it is the highest peak in the reference sensor measurements. However, in the sensor unit measurement, the natural frequency peak is visible, but amplitude is low compared to the other peaks.

Figure 7 b) presents the raw u-axis acceleration data of the same EBSC measurement and Figure 7 a) presents the coordinate transformed data shown in the Figure 5 a). In the raw acceleration data, the vibration frequencies are presented as two peaks (sidebands), which are approximately 16.6 Hz (two times the rotation frequency, 8.3 Hz) apart from each other. The average of the peaks is the frequency measured from the bearing housing or observed after the coordinate transformation. The phenomenon is caused by an amplitude modulation. Because the sensor is rotating with the rotor, the direction of the sensor axes changes in the Earth's coordinate system. However, the vibration direction stays constant in the Earth's coordinate system, which causes the vibration amplitude to modulate in the sensor coordinate system depending of the sensor angle in the Earth's coordinate system. The amplitude change occurs at the rotation frequency, which causes the sidebands to appear at both sides of the vibration frequency with an offset of rotation frequency.

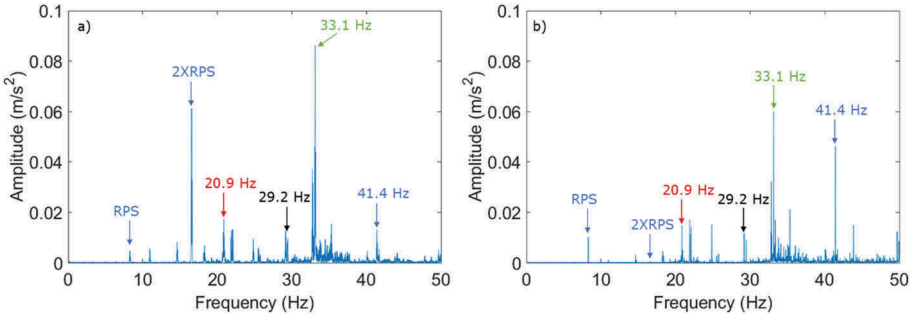

Figure 5. Horizontal (x-axis) vibration at 500 rpm (8.3 Hz) in the frequency domain. a) Sensor unit measurement with the encoder-based sample clock and b) reference sensor measurement from the bearing housing. RPS means rounds per second, which is equal to the rotation frequency.

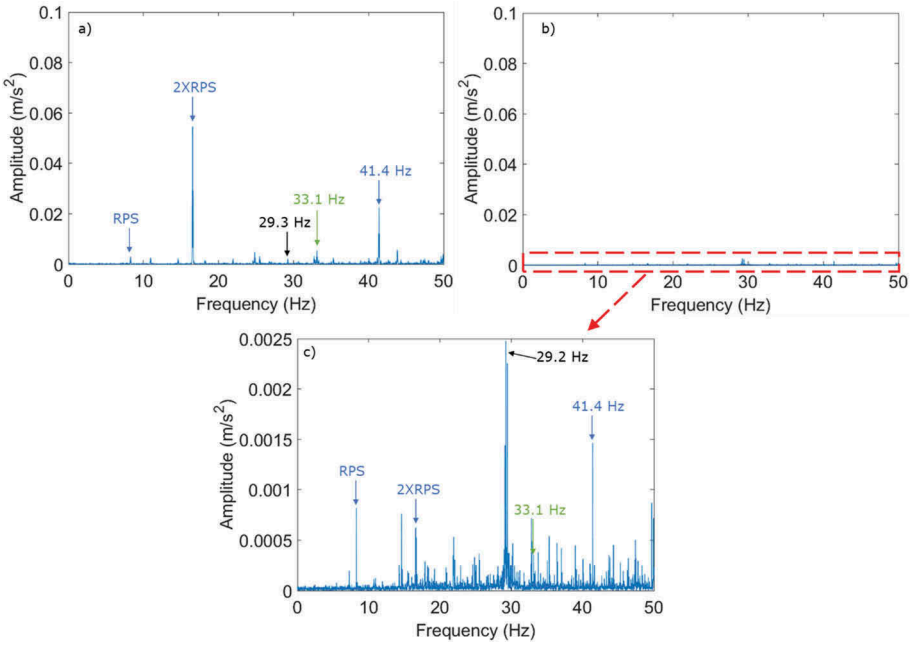

Figure 6. Vertical (y-axis) vibration at 500 rpm (8.3 Hz) in the frequency domain. a) Sensor unit measurement with the encoder-based sample clock, b) reference sensor measurement from the bearing housing with the same y-axis scale as in a) and c) scaled plot from the reference sensor measurement. RPS means rounds per second, which is equal to the rotation frequency.

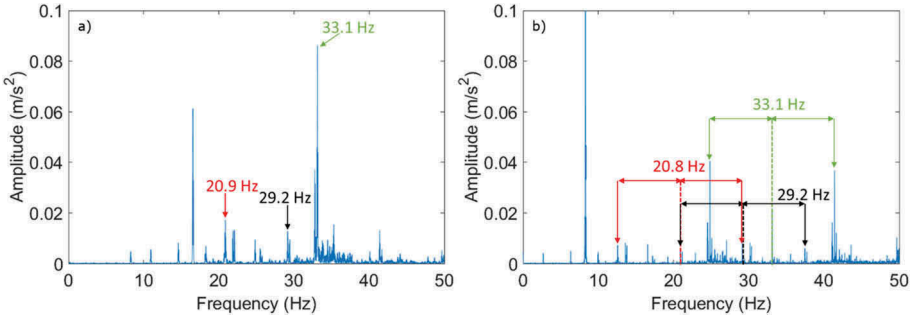

Figure 7. Comparison between horizontal coordinate transformed and raw u-axis sensor unit data in the frequency domain from the encoder-based sample clock measurement. a) horizontal coordinate transformed data and b) raw u-axis sensor unit data. The averages of the marked frequency peaks in b), are the same values as in the coordinate transformed data. The values presented in b), are the average of the frequency peaks where the same colored arrows point. This is caused by an amplitude modulation of the measured signal due to the sensor rotating.

3.2 Time-based sample clock measurement

Figures 8 and 9 present the same data from the EBSC measurement as in Figures 5 and 6, and the measurement data from the TBSC measurement, with the gravity-based phase, after the coordinate transformation. Some peaks can be observed in both figures in the vertical and horizontal directions. Most significant differences occur at the rotation frequency and two times rotation frequency. In the horizontal vibrations, the amplitude of the two times rotation frequency is significantly lower in the EBSC measurement than in the TBSC. In the vertical vibrations, the magnitudes of the amplitude differences were not as high.

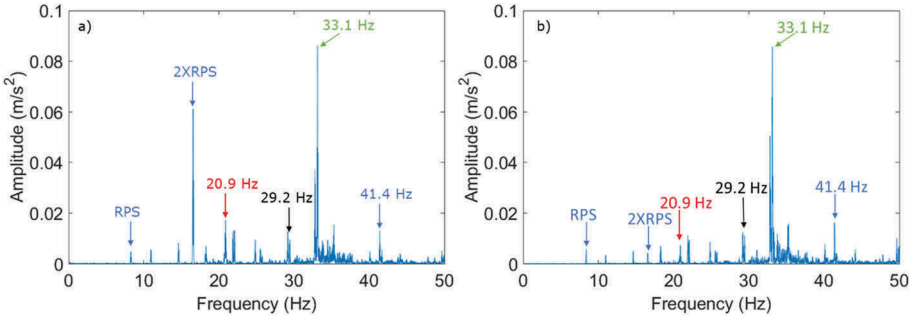

Figure 8. Horizontal (x-axis) vibration at 500 rpm (8.3 Hz) in the frequency domain. a) Sensor unit measurement with the encoder-based sample clock and b) sensor unit measurement with the time-based sample clock. RPS means rounds per second, which is equal to the rotation frequency.

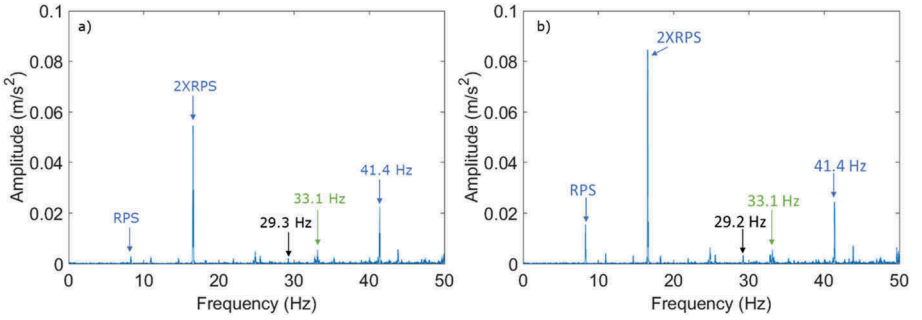

Figure 9. Vertical (y-axis) vibration at 500 rpm (8.3 Hz) in the frequency domain. a) Sensor unit measurement with the encoder-based sample clock and b) sensor unit measurement with the time-based sample clock. RPS means rounds per second, which is equal to the rotation frequency.

3.3 Comparison of phase calculating methods

Figure 10 presents the phase difference between the two different methods for calculating the phase: one that utilized the encoder and one that utilized the gravitational components of the MEMS sensor data. Both methods were applied to the 500 rpm EBSC measurement. The phase was constantly shifted approximately 1.9 degrees, and

there was an oscillation in the form of a sine wave. It was assumed that the encoder based phase determination was correct; this suggests that gravity-based phase determination lags ca 1.9 degrees and has oscillation in the range of 1-2.5 degrees.

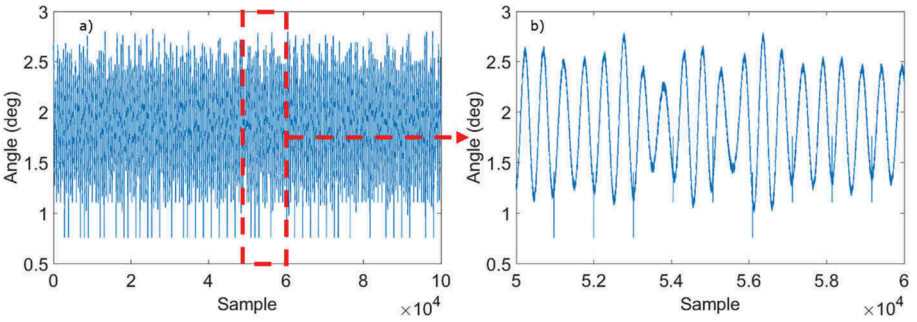

Figure 10. Difference of encoder-based sample clock sensor unit measurement with both phase calculation methods. a) is from 100000 samples and b) is a closeup of 50000 to 60000 samples. The x-axis is the sample count of the measurement.

Figure 11 presents the horizontal vibration of the data of the EBSC measurement with both phase-calculating methods. Figure 11 a) presents the results with the encoder-based phase and Figure 11 b) presents the results with the gravity-based phase. Similar results can observe as in Figure 8: the most significant difference appears in the amplitude of the two times rotation frequency (2XRPS, 16.6 Hz) peak. However, there is an amplitude difference in the horizontal natural frequency as well. Nevertheless, both methods present the same frequency peaks, even though there was a small difference in the phases depending on the calculating method.

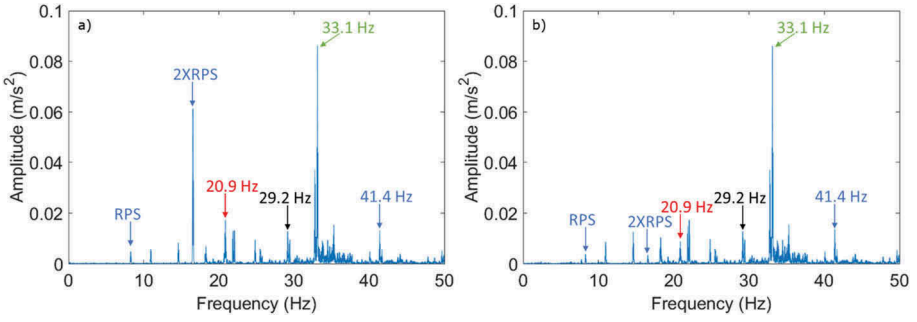

Figure 11. Horizontal vibration of the 500 rpm encoder-based sample clock measurement in the frequency domain. a) presents the results of a coordinate transformation made with the encoder-based phase and b) presents the results of coordinate transformation made with the gravity-based phase.

4 DISCUSSION

The results showed that it is possible to separate the horizontal acceleration data from the rotating sensor data; however, there were some difficulties in separating the vertical data. The reason for this may be that the amplitudes of the signal in vertical direction were significantly lower. The lower amplitudes can be observed from the reference measurement from the bearing housing. The highest amplitude in the vertical direction was approximately 0.0025 m/s^2 when in the horizontal direction, it was approximately 0.06 m/s^2. The amplitude differences are caused by the different stiffnesses in the vertical and horizontal directions of the test bench foundation. In the vertical direction, there were some of the same frequency peaks, which were observed in the horizontal direction. The higher magnitude vibration of the horizontal direction may have caused the vibrations to be visible in the vertical direction as well. However, the horizontal natural frequency is not visible in the vertical data, which indicates that the separation of the vertical data from the horizontal one may be possible. Nevertheless, the horizontal results were promising. Both on-shaft and reference sensors observed the same frequency peaks.

The comparison between the TBSC and EBSC sensor unit measurements showed that no significant differences occur depending on the sampling clock method. The most significant differences appear in the amplitudes of the rotation frequency and at twice the rotation frequency. The reason for that may be the different methods for calculating the phase. The horizontal natural frequency (20.9 Hz) can be observed from both figures. The vertical natural frequency can be observed from both measurements as well, but the amplitudes are quite low. However, if the vertical natural frequency peak amplitudes of the time and encoder-based sample clock sensor unit data is compared to the amplitude of the reference measurement, they are in the same range. The EBSC measurement, TBSC measurement and the reference measurement have a vertical natural frequency amplitude of 0.0020 m/s^2, 0.0033 m/s^2, and 0.0025 m/s^2, respectively. However, the reference sensor and proposed sensor unit were mounted to different parts of the machine, which may affect the amplitudes.

The results showed a promising start for separating the horizontal and vertical vibration of a rotating two-axis accelerometer. The horizontal vibration was separated well from the raw measurement data; however, the vertical vibration was not as clear as the horizontal. Hence, separating the vertical and horizontal vibration needs to be studied more, and one way to do it is to use the sensor unit in a test rotor bench were the magnitude of the vertical and horizontal vibrations are more similar to each other.

Still in many applications, the accelerometer mounted to the static part of the machine is better way of measuring the machine vibrations. However, in some machines it is not possible to measure the vibrations effectively from a static part of the machine. In these applications, on-shaft accelerometers could be used. On-shaft accelerometers also opens new possibilities to study machine condition monitoring and to measure other aspects of machines such as, lateral vibrations or central point movement. Lateral vibrations could be measured from the rotor, if the accelerometer is mounted with a small offset from the central axis. This would be a cost-effective method to measure the lateral vibrations with minimal measurement setup process. The central point movement is typically not measured in rotating machines because it is expensive, or the measurement instruments cannot fit close enough to the rotating part. The sensor unit could be mounted inside of a rotor or even several places in one rotor. This way, the central point movement could be determined from different positions of the rotor and find the modal shapes affecting it.

5 CONCLUSION

This study presents a novel on-shaft sensor unit with a MEMS accelerometer, inverse encoder and wireless data transfer. The encoder rotates with the rotor, and the encoder shaft i.e. code wheel is mounted to the static part of the machine. The light sensors measuring the code wheel are rotating with the rotor, hence enabling to use of the encoder pulse as a sample clock without slip rings. The sampling can also be clocked with time, which enables testing of gravity-based phase calculation and comparing the result to the encoder-based phase calculations. There were some differences in the phases with the different calculating methods. However, when the coordinate transformation was made with the different phases, the results did not differ significantly.

The separation of the horizontal and vertical axis from the data of the rotating sensor showed promising results. The horizontal vibration was well visible from the data and presented the same vibration peaks, as did the reference measurement. However, the vertical vibration did not occur as clearly as it did in the reference measurement; hence the presented method needs more research.

ACKNOWLEDGEMENTS

This research was supported by Academy of Finland (Digital Twin of Rotor System, under Grant 313675) and Business Finland (Reboot IoT Factory, under Grant 4356/31/2019).

REFERENCES

[1] A. Albarbar, S. Mekid, A. Starr, and R. Pietruszkiewicz, "Suitability of MEMS Accelerometers for Condition Monitoring: An experimental study," *Sensors*, vol. 8, pp. 784–799, 2008.

[2] A. Albarbar, A. Badri, J. K. Sinha, and A. Starr, "Performance evaluation of MEMS accelerometers," *Measurement: Journal of the International Measurement Confederation*, vol. 42, no. 5, pp. 790–795, 2009.

[3] J. D. Son, B. H. Ahn, J. M. Ha, and B. K. Choi, "An availability of MEMS-based accelerometers and current sensors in machinery fault diagnosis," *Measurement: Journal of the International Measurement Confederation*, vol. 94, pp. 680–691, 2016.

[4] I. Koene, R. Viitala, and P. Kuosmanen, "Internet of Things Based Monitoring of Large Rotor Vibration With a Microelectromechanical Systems Accelerometer," *IEEE Access*, vol. 7, pp. 92210–92219, 2019.

[5] I. Koene, R. Viitala, and P. Kuosmanen, "Vibration analysis of a large rotor over industrial internet," in *59th Ilmenau Scientific Colloquium*, pp. 1–9, 2017.

[6] A. Vogl, D. T. Wang, P. Storås, T. Bakke, M. M. V. Taklo, A. Thomson, L. Balgård, "Design, process and characterisation of a high-performance vibration sensor for wireless condition monitoring", *Sensors and Actuators A: Physical*, vol. 153, pp. 155–161, 2009.

[7] C. Acar, A. Shkel, "Experimental evaluation and comparative analysis of commercial variable-capacitance MEMS accelerometers", *Journal of Micromechanics and Microengineering*, vol. 13, pp. 634–645, 2003.

[8] A. Aydemir, Y. Terzioglu, T. Akin, "A new design and a fabrication approach to realize a high performance three axes capacitive MEMS accelerometer", *Sensors and Actuators, A: Physical*, vol. 244, pp. 324–333, 2016.

[9] B. Tang, K. Sato, S. Xi, G. Xie, D. Zhang, Y. Cheng, "Process development of an all-silicon capacitive accelerometer with a highly symmetrical spring-mass structure etched in TMAH + Triton-X-100", *Sensors and Actuators A: Physical*, vol. 217, pp. 105–110, 2014.

[10] Z. Mohammed, G. Dushaq, A. Chatterjee, M. Rasras, "An optimization technique for performance improvement of gap-changeable MEMS accelerometers", *Mechatronics*, vol. 54, pp. 203–216, 2018.
[11] Y. J. Chan and J.-W. Huang, "Multiple-point vibration testing with micro-electromechanical accelerometers and micro-controller unit," *Mechatronics*, vol. 44, pp. 84–93, 2017.
[12] M. E. Elnady, J. K. Sinha, and S. O. Oyadiji, "Identification of Critical Speeds of Rotating Machines Using On-Shaft Wireless Vibration Measurement," *Journal of Physics: Conference Series*, vol. 364, pp. 1–10, 2012.
[13] M. E. Elnady, A. Abdelbary, J. K. Sinha, and S. O. Oyadiji, "FE and Experimental Modeling of On-shaft Vibration Measurement," in *Proceedings of the 15th International Conference on Aerospace Sciences & Aviation Technology*, no. May, pp. 1–18, 2013.
[14] S. Jiménez, M. O. T. Cole, and P. S. Keogh, "Vibration sensing in smart machine rotors using internal MEMS accelerometers," *Journal of Sound and Vibration*, vol. 377, pp. 58–75, Sep. 2016.
[15] G. Feng, N. Hu, Z. Mones, F. Gu, and A. D. Ball, "An investigation of the orthogonal outputs from an on-rotor MEMS accelerometer for reciprocating compressor condition monitoring," *Mechanical Systems and Signal Processing*, vol. 76–77, pp. 228–241, Aug. 2016.
[16] O. O. Esu, J. a Flint, and S. J. Watson, "Condition Monitoring of Wind Turbine Blades Using MEMS Accelerometers," *Renewable Energy World Europe*, pp. 1–12, 2013.
[17] M. Mollineaux, K. Balafas, K. Branner, P. Nielsen, A. Tesauro, et al., "Damage Detection Methods on Wind Turbine Blade Testing with Wired and Wireless Accelerometer Sensors," EWSHM - 7th European Workshop on Structural Health Monitoring, IFFSTTAR, Inria, Université de Nantes, Nantes, France, 2014.
[18] R. Simon Carbajo, E. Simon Carbajo, B. Basu, and C. Mc Goldrick, "Routing in wireless sensor networks for wind turbine monitoring," *Pervasive and Mobile Computing*, vol. 39, pp. 1–35, Aug. 2017.
[19] G. Kilic and M. S. Unluturk, "Testing of wind turbine towers using wireless sensor network and accelerometer," *Renewable Energy*, vol. 75, pp. 318–325, 2015.
[20] J. W. Cooley and J. W. Tukey, "An Algorithm for the Machine Calculation of Complex Fourier Series," *Mathematics of Computation*, vol. 19, no. 90, p. 297, 1965.